Document-131188

Design Note TRI-DN-16-09
CANREB HRS Multipole Corrector

Document Type: Design Note

Release: 1 **Release Date:** 2016-04-14

Author(s): Jim A. Maloney

	Name:	Signature
Author:	Jim A. Maloney	APPROVAL RECORD
Reviewed By:	Marco Marchetto	
	Friedhelm Ames	
Approved By:	Rick Baartman	
	Reiner Kreucken	

Note: Before using a copy (electronic or printed) of this document you must ensure that your copy is identical to the released document, which is stored on TRIUMF's document server.

History of Changes

Release Number	Date	Description of Changes	Author(s)
#01	2016-04-14	Initial release	J.A. Maloney

Keywords: HRS, CANREB, Multipole Corrector

Distribution List: Jim A. Maloney, Marco Marchetto, Rick Baartman, George Clark, Eric Guetre, Mike Rowe, Friedhelm Ames, Reiner Kruecken, Asita Perera

1 Abstract

To meet the requirements described in the ARIEL High Resolution Spectrometer Requirements (Document-74319), and the ARIEL High Resolution Separator (HRS) Design Note - TRI-DN-14-06 (Document-109442), the design for an electrostatic corrector is detailed. This corrector can create specific 2n-pole electric field harmonics from 4-pole (quadrupole) up to 12-pole (duodecapole). These will allow for correction of non-linear optical effect in the HRS beamline, leading to improve resolution and transmission through the HRS.

2 Introduction

2.1 Purpose

The purpose of this design note is to provide the basic information detailing the design and functioning of the HRS electrostatic multipole corrector. This will serve as a basis for future technical drawings concerning the corrector. This note will also describe the corrector's intended operation.

2.2 Scope

This design note describes the conceptual and optimized design for the HRS electrostatic multipole corrector.

2.3 Definitions and Abbreviations

1. HRS: High resolution separator (or spectrometer). The HRS is a component in the scope of the CANREB project.
2. CANREB: CANadian Rare-isotope facility with Electron-Beam ion source project. CANREB is part of the ARIEL program.
3. ARIEL: Advanced Rare IsotopE Laboratory program.
4. COSY: Beamline simulation code COSY Infinity Version 9.1 updated January 2013 [1].
5. OPERA: OPERA-3D is a simulation code for designing and modelling electromagnetic elements from COBHAM/Vector Fields [2].

3 Overview of Nonlinear Beam Optics

The optical design of the HRS is described in detail in TRI-DN-14-06. The HRS consists of a pair of 90-degree magnetic dipoles, and an upstream and downstream matching section. Two additional electrostatic quadrupoles are located between the waist slits and the magnets. Between the "waist" slit apertures, shown below in Figure 1, the beam is imaged in horizontal phase space. This imaging is based on a linear model where elements in the beamline are approximated using matrices to describe particle coordinates within the beam and how those coordinates evolve from an initial to a final state. While this approach is sufficient for an initial conceptual beamline design, a more accurate picture is needed to insure the resolution and transmission requirements for the HRS will be met.

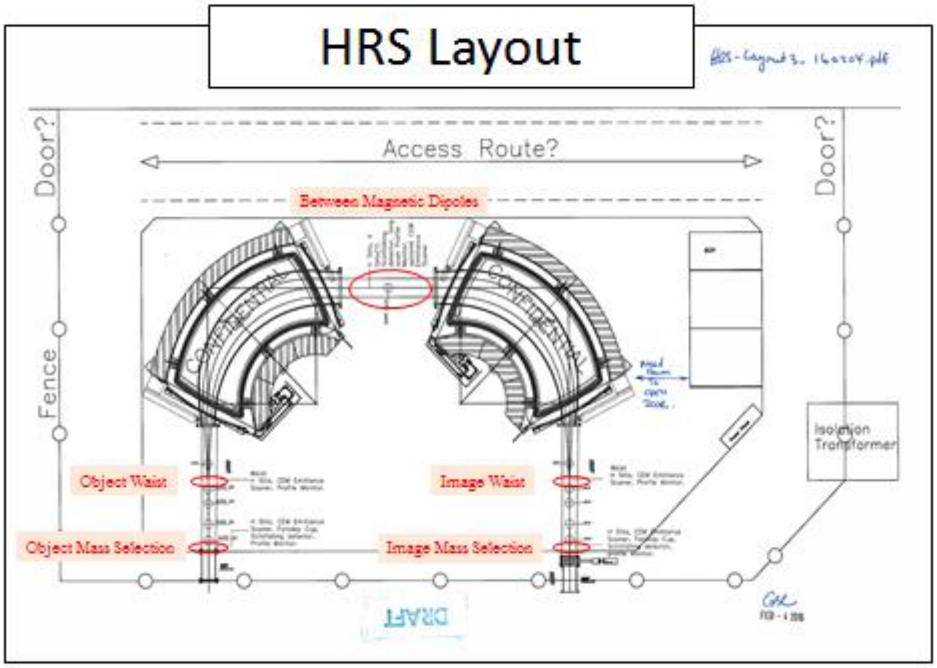

Figure 1: HRS layout schematic.

For example, the electrostatic potential of a quadrupole is often expressed in cylindrical coordinates (where z is aligned along the optical axis of the element):

$$V_E = M_{2,2}(z)\cos(2\varphi)\, r^2 \tag{1}$$

where $M_{2,2}(z)$ represents the strength function.

This approximation is not physical. Satisfying Laplace's equation ($\nabla^2 V_E = 0$) requires the addition of higher order terms because the potential will falloff in the fringe field region entering and exiting the element [3, 4]. In the case of the electrostatic quadrupole, for example, the potential can be expressed with the lowest order correction:

$$V_E = M_{2,2}(z)\cos(2\varphi)\, r^2 - M''_{2,2}(z)\cos(2\varphi)\, r^4/12 \tag{2}$$

COSY calculates these terms to arbitrary order, allowing the user to identify how these nonlinear terms effect the beam optics. COSY describes, by use of a Taylor expansion, how the initial coordinates of a particle within the beam, affect its final coordinates.

In the HRS, a particularly large second order nonlinear effect is corrected in the HRS optical design by introduction of a curvature to the entrance and exit edges of the dipole magnets. An alternative method would be to use a sextupole.

The function of the electrostatic multipole corrector being designed in this note is to provide a mechanism for correction of the nonlinearities resulting from other elements in the HRS beam line. It can be used, for example, as a fine tune to the second order correction being made via the dipole edge curvatures, and also as an independent means of correction for other higher order aberrations.

To illustrate this effect, Figure 2(a) shows how nonlinear effects distort the horizontal phase space image for two masses separated by 1:20000 between the entrance and exit of the pure separator section of the HRS even with the optimal edge curvature correction. A multipole corrector located between the two bending dipoles corrects the final image, as shown in Figure 2(b), using an octupole harmonic.

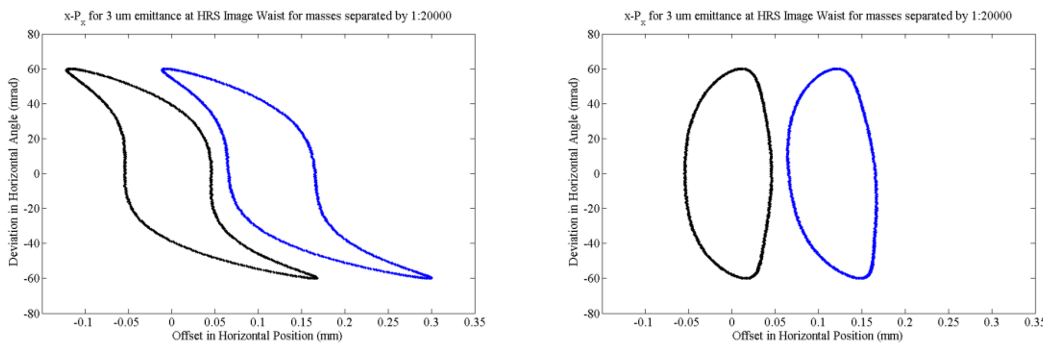

Figure 2 (a-b): Horizontal phase space at the HRS waist image for masses differing by 1:20000 based on 5^{th} order COSY simulation (a) without multipole correction, and (b) using multipole for correction 3^{rd} order nonlinearities.

4 Electrostatic Multipole Map Modelling

COSY provides internal functions for modelling most beam line elements. It also allows the user to approximate the form of the falloff for entrance and exit fringe fields using a 6-parameter ENGE function. Two concerns exist, however, with relying on these internal functions. First, the functions tend to be idealized and adjusting them to include effects such as field clamps and grounding plates is not a simple task. For example, in the 24-pole squirrel-cage multipole model discussed below, the physical arrangement of the poletip in the OPERA model do not produce a symmetric decapole (poletips of alternating voltage arranged radially every 36 degrees) like the one modelled in the COSY internal function. Additionally, there is a concern for how COSY treats fringe fields for short elements. In calculating the fringe field, COSY begins by applying a negative length drift and integrating through the element. The process is reverse for the exit fringe field. While this is fine for long elements, where the fields reach a maximum at some position inside the element, in the case of short elements the entrance and exit fields can overlap. This makes the higher order calculations subject to question. This effect is illustrated in Figure 3(a-b) below which shows the longitudinal falloff for a 500 mm vs 100 mm long sextupole with a 17.5 cm radial aperture.

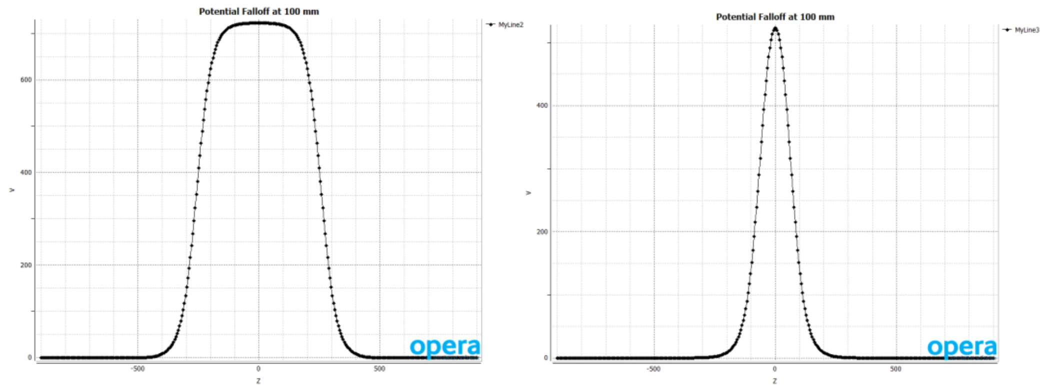

Figure 3(a-b): Longitudinal potential falloff for sextupole with 15 cm radial aperture along a trajectory offset by 10 cm horizontal to the optical axis for sextupole of length (a) 500 mm and (b) 100 mm.

Using a modified procedure for COSY Infinity [5, 6], electrostatic beamline elements can be modelled from a mid-plane map of the potential. This process addresses both of the concerns previously mentioned. For example, using OPERA, a cylindrical sextupole was created, including grounding plates and vacuum chamber. The electric potential on a grid of points in the midplane was produced and compared to the internal model of a sextupole in COSY. The output transfer maps, shown to second order in Table 1, were comparable. The poletip strength of the sextupole can be matched to the OPERA model by simply scaling the map data. The critical transfer map terms (a|xx) (a|yy) and (b|xy) are marked for comparison.

Table 1: 2nd Order COSY Transfer Maps for COSY Internal Sextupole Model (EH) and OPERA Model of the Element Using Midplane Electric Potential Data (MELP)

Map with EH

1.000000	0.000000	0.000000	0.000000	0.000000	100000
0.3000000	1.000000	0.000000	0.000000	0.000000	010000
0.000000	0.000000	1.000000	0.000000	0.000000	001000
0.000000	0.000000	0.3000000	1.000000	0.000000	000100
0.000000	0.000000	0.000000	0.000000	1.000000	000010
0.000000	0.000000	0.000000	0.000000	0.7499998E-01	000001
-0.1464908	-0.9766054	0.000000	0.000000	0.000000	200000
-0.7410816E-02	-0.2929816	0.000000	0.000000	0.000000	110000
-0.5558112E-03	-0.4024184E-01	0.000000	0.000000	-0.7500001E-01	020000
0.000000	0.000000	0.2929816	1.953211	0.000000	101000
0.000000	0.000000	0.7410816E-02	0.2929816	0.000000	011000
0.1464908	0.9766054	0.000000	0.000000	0.000000	002000
0.000000	0.000000	0.7410816E-02	0.2929816	0.000000	100100
0.000000	0.000000	0.1111622E-02	0.8048367E-01	0.000000	010100
0.7410816E-02	0.2929816	0.000000	0.000000	0.000000	001100
-0.1500000	0.000000	0.000000	0.000000	0.000000	010001
0.5558112E-03	0.4024184E-01	0.000000	0.000000	-0.7500001E-01	000200
0.000000	0.000000	-0.1500000	0.000000	0.000000	000101
0.000000	0.000000	0.000000	0.000000	-0.5624999E-01	000002

```
Map with MELP
   1.000000     0.4810097E-05  0.000000      0.000000    -0.3748613E-04 100000
  0.3000001      1.000001      0.000000      0.000000    -0.5622919E-05 010000
   0.000000      0.000000     0.9999997   -0.3783820E-05  0.000000      001000
   0.000000      0.000000     0.2999999     0.9999992     0.000000      000100
   0.000000      0.000000      0.000000      0.000000     1.000000      000010
  0.5622920E-05 0.3748613E-04  0.000000      0.000000     0.7499997E-01 000001
 -0.1464904    -0.9766032      0.000000      0.000000     0.2918144E-05 200000
 -0.3094920E-01-0.2929810      0.000000      0.000000     0.5137372E-06 110000
 -0.2321191E-02-0.2847256E-01  0.000000      0.000000    -0.7500000E-01 020000
   0.000000      0.000000     0.2927101      1.951401     0.000000      101000
   0.000000      0.000000     0.3099961E-01 0.2927103     0.000000      011000
  0.1463551      0.9757011     0.000000      0.000000    -0.2662233E-05 002000
   0.000000      0.000000     0.3107458E-01 0.2927103     0.000000      100100
   0.000000      0.000000     0.4661188E-02 0.5681348E-01  0.000000      010100
  0.3099962E-01 0.2927103      0.000000      0.000000    -0.5148555E-06 001100
 -0.7499076E-06-0.5836293E-05  0.000000      0.000000     0.3748612E-04 100001
 -0.1500002    -0.1722495E-05  0.000000      0.000000     0.5622918E-05 010001
   0.000000      0.000000     0.5986540E-06 0.5324468E-05  0.000000      001001
  0.2319348E-02 0.2836925E-01  0.000000      0.000000    -0.7500001E-01 000200
   0.000000      0.000000    -0.1499998     0.1566259E-05  0.000000      000101
 -0.5622921E-05-0.1874308E-04  0.000000      0.000000    -0.5624998E-01 000002
 ------------------------------------------------------------------------------
```

The Columns 1-5 represent the coefficient in the Taylor series for the final coordinate x, a, y, b, d, and the 6th column lists the exponential dependence based on the initial coordinates x, a, y, b, l, d. For example, the first highlighted term in the second column represents the (a|xx) coefficient. A more detailed explanation of COSY's coordinate system and the transfer map out are discussed in [7].

Next, the pure separator portion of the HRS was modeled in COSY showing the correct dipole edge curvature to correct second order nonlinearities, and also with a 1 cm variation in the radius of the edge curvature. The effect of this error and all other uncorrected nonlinearities through 5th order is shown in Figure 4. Similar errors can also be introduced due to misalignment of the dipoles. One of the functions of the electrostatic corrector is to compensate for this error as well and address uncorrected higher order nonlinearities in the beam optics.

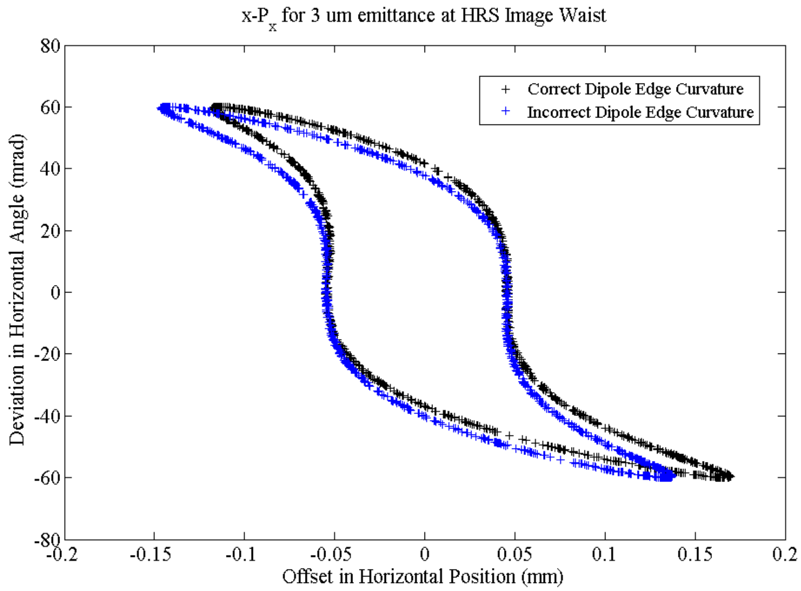

Figure 4: Horizontal phase space variation at HRS Image Waist due to error in dipole edge curvature.

Both the COSY internal sextupole and the OPERA map-based model where then used to attempt to correct the 2nd order aberrations shown in Figure 4. For the internal element, the poletip strength was fit, and for the OPERA map-based element, the scaling parameter for the map data was fit. A voltage of ~2.2 V was needed for at the poletip for an aperture radius of 0.2 m. The results, including the residual 3rd order and higher nonlinearities, are shown in Figures 5(a-b). The process was repeated for the octupole, as shown in Figures 6(a-b), showing the consistency between the OPERA and COSY models of the corrector. For the octupole correction, a poletip voltage of ~15.5 V was needed for an aperture radius of 0.2 m. This process can also be applied to higher order modes of the corrector. The potential map for the combined function corrector is merely a summation of these multipole modes. This same potential map method was also used to study the more sophisticated Squirrel-Cage and Novel multipole correctors discussed below.

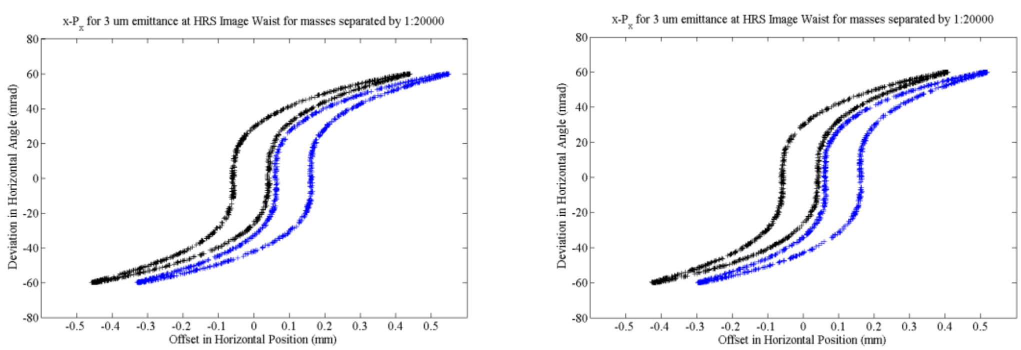

Figure 5(a-b): Horizontal Phase Space at HRS Image Waist with only 2nd order correction for two masses that differ by 1:20000 (a) using COSY's internal sextupole model, and (b) using midplane potential map date from OPERA sextupole model.

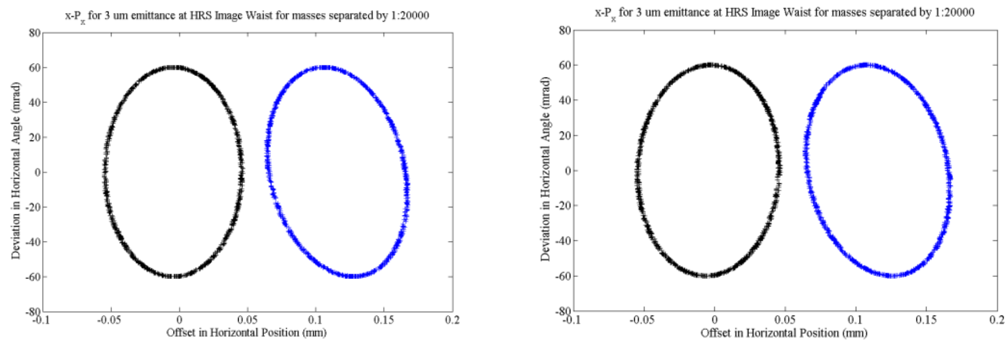

Figure 6(a-b): Horizontal Phase Space at HRS Image Waist for two masses differing by 1:20000 with correction through 3rd order (a) using COSY's internal octupole model, and (b) using midplane potential map date from OPERA sextupole model.

5 Squirrel-Cage Model

An initial model for the corrector was developed and discussed in the HRS Design Note based on a technical drawing of the so-called squirrel-cage design being used at the CARIBU facility [8]. The corrector, based on the HRS optic design, will function primarily as an octupole. A sextupole mode is required to address machining errors in the dipole edge angle or alignment errors in the dipoles, and decapole and duodecapole modes were also desired. To facilitate this, an arrangement of 24 cylindrical poletips was chosen.

In between the magnetic dipoles, the beam envelope of a 3 um emittance is approximately +/- 10 cm from the optical axis. This size increases to approximately +/- 13.5 cm for an emittance of 6 um. The vertical beam size is only on the order of approximately +/- 2.5 mm in both cases. Envelope plots are provided in Appendix B for reference. The inner radial aperture of 17.5 cm was chosen to give ample horizontal clearance for the beam. The length of the corrector was arbitrarily chosen as 30 cm. The structure is surrounded by a ground-box, including shunts to limit the length of the fringe field extending from the corrector. A wire-frame rendering of this model and the ground-box surrounding it is shown in Figure 7.

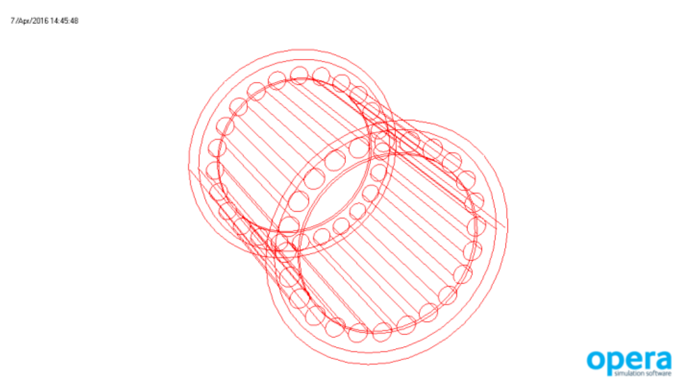

Figure 7: Wireframe rendering of the squirrel-cage model for the HRS multipole.

The model was also simulated with a vacuum chamber, including rectangular to cylindrical flanges, as shown in Figure 8.

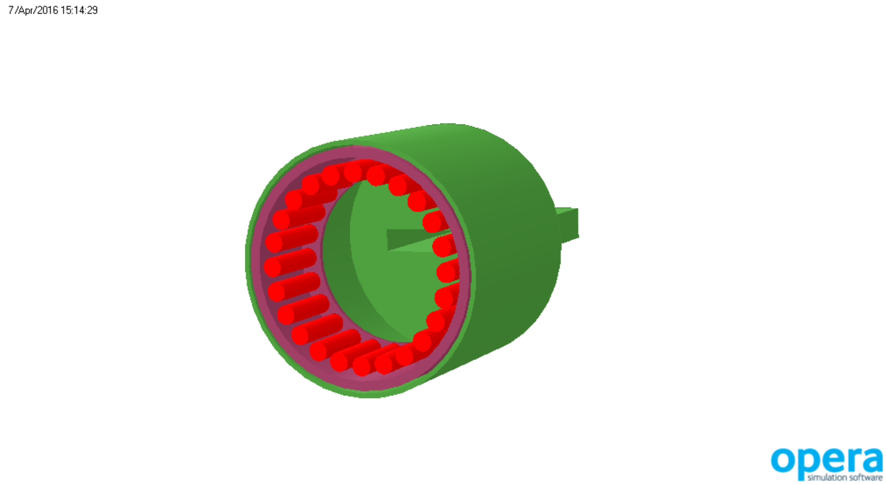

Figure 8: ½ cutaway view of OPERA Model of squirrel-cage correction and vacuum chamber.

Figures 9(a-b) shows the effect of the model with and without the shunts (an end cap to the groundbox with a radial aperture of 17 cm). Limiting the length of the fringe field region helps to minimize interaction with the magnetic dipole fringe fields as well as other beamline components such as diagnostics or the vacuum chamber flanges.

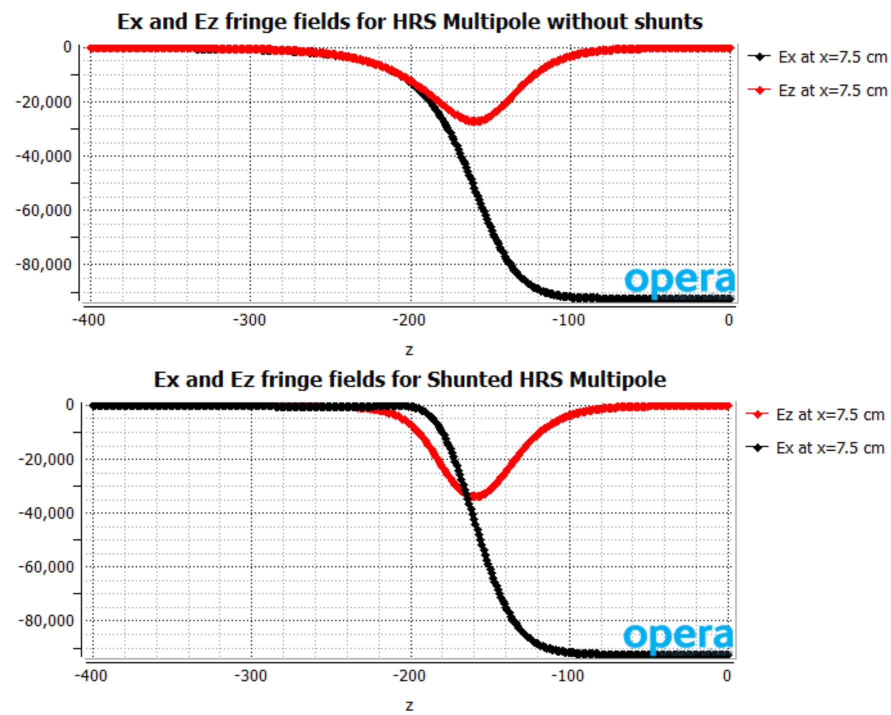

Figure 9(a-b): Comparison of falloff in electric fields for HRS corrector model (a) with (top) and (b) without (bottom) shunts added to the ground-box. Z = 0 represents the geometric center of the 30 cm long corrector.

The functioning of this design is well understood. The poletips are powered to produce the multipole mode desired (or combination thereof), taking advantage of the cylindrical symmetry. For example, if every other one of the 24 poletips is powered with alternating voltages, a duodecapole mode is produced. The potential can also be split between adjacent poles to optimize the equipotential contour. In the case of a sextupole, as shown in Figure 10 for example, instead of charging only every 4th poletip, the voltage can be distributed to the adjacent poletips. Shaping the equipotential surface this way allows for minimization of the next higher order correction in the multipole expansion [9, 10]. An example of how the poletips are powered proportionally for different modes is listed in Appendix A.

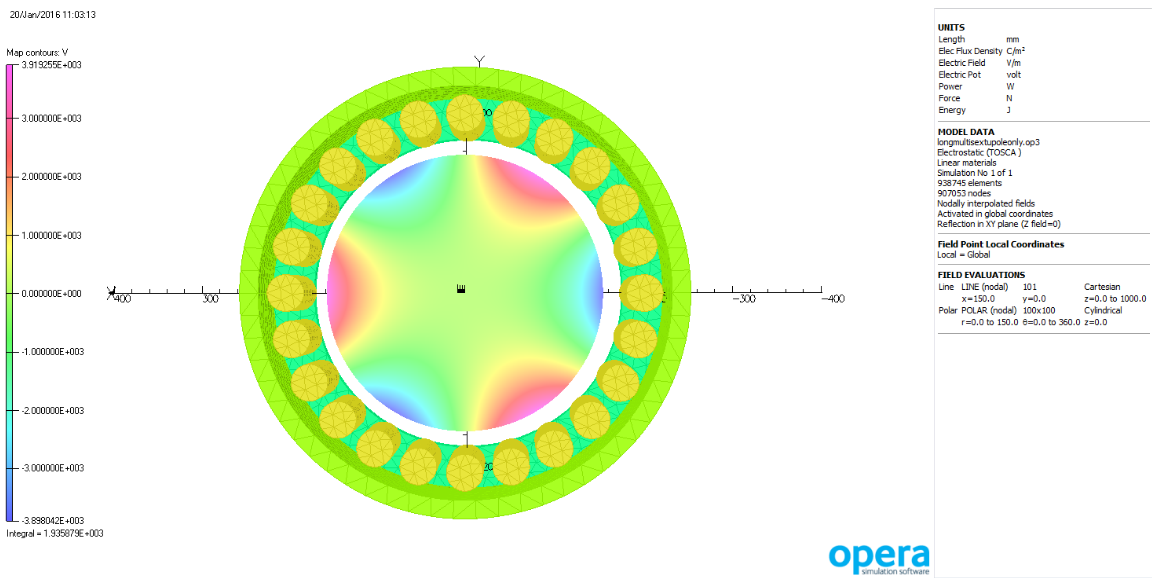

Figure 10: Profile of the electric potential for the sextupole mode of the squirrel-cage corrector.

In the design shown above, the poletips have a 2 cm radius and are centered 19.5 cm from the optical axis. This spacing is important since higher order modes can be felt closer to the poletips as shown in Figure 11 below. As you move farther out radial from the optical axis, the potential deviates from the $V_E = M_{3,3}(z)\cos(3\varphi)\,r^3$ multipole expansion formula we expect for an ideal sextupole. The geometry chosen in this model remains close to the ideal form up to the expected horizontal beam envelope of ~ 10 cm. Minimizing the spacing between the poletips (by increasing their radius) also helped to reduce this effect. A comparison of the OPERA model and the ideal potential function along the horizontal line in the geometric center of the element is shown in Figure 12.

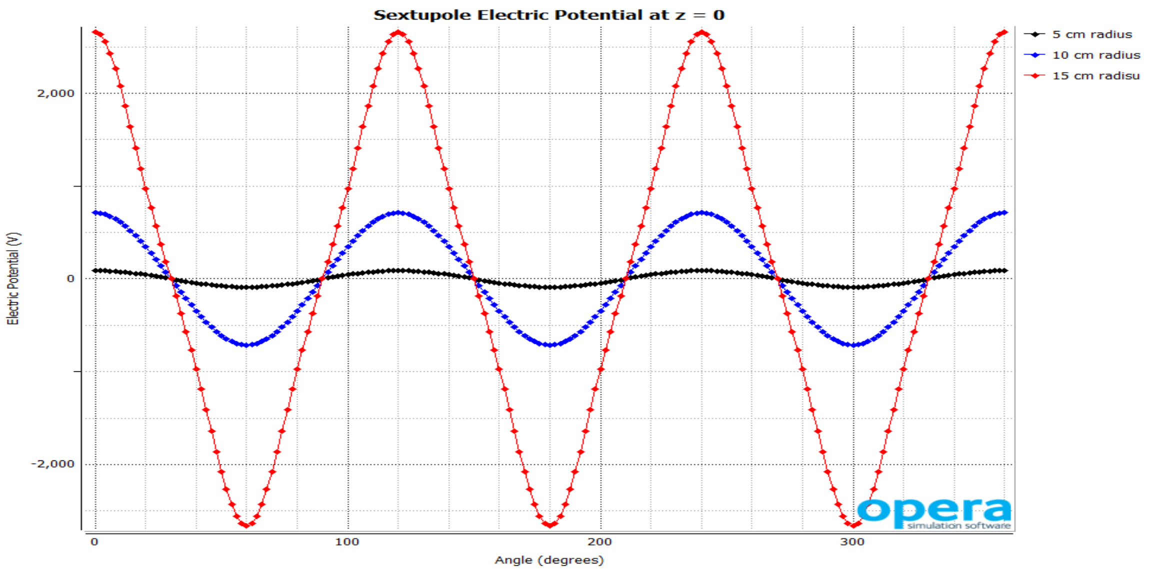

Figure 11: Radial variation in the electric potential for the squirrel-cage model in sextupole mode (z = 0 represents the geometric center of the corrector).

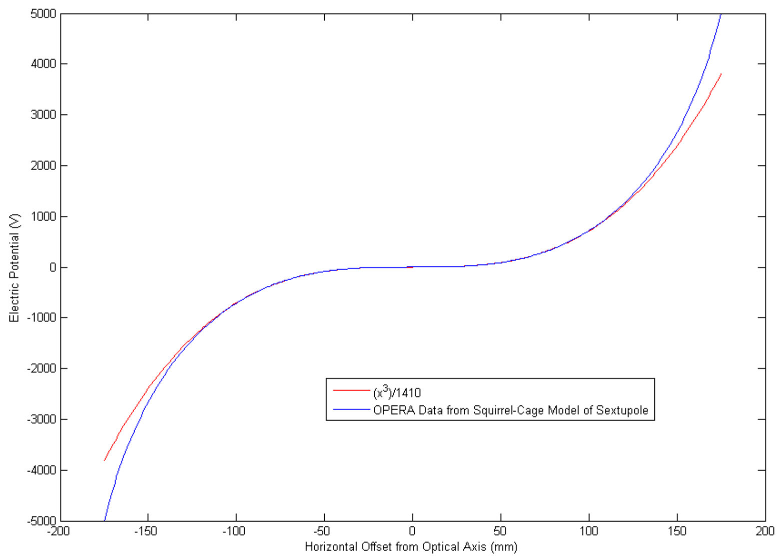

Figures 12: Comparison of squirrel-cage OPERA corrector to ideal sextupole along a horizontal line in the midplane in the center of the corrector (y = z = 0).

Because the initial choice for the length of the multipole was arbitrary, a study was done to determine if element length affected the optics of the corrector. These simulations included the vacuum chamber and flange located based on best information available [11]. Ultimately, there was no appreciable difference in the transfer maps produced by COSY for models ranging from as short as 100 mm to as long as 500 mm. The advantage to a shorter multipole is that it allows more space for diagnostic elements to be placed between the magnetic dipoles. A shorter multipole would, however, require higher voltages on the poletips to achieve the same integrated field. The corrector should be designed in a manner that makes all external wiring invisible to the beam. Given the number of power supplies and leads that need to be fed into the corrector poletips, this would be more complicated with a shorter corrector. As a result of these considerations, the 30 cm length remains the default choice for this model, subject to revision when engineering drawings are prepared.

The number and type of power supplies are not specified in this note. Based on the radial aperture of this model and the optic design [12], in the optimal case little or no sextupole correction is necessary. From octupole through duodecapole, the voltages at the poletip range from ~15 V to ~1.31 V, respectively. Simulations for "worse case" alignment and machining errors in the magnetic dipoles could require a sextupole with poletip voltages of about 1 kV. Ideally, the power supplies should be capable of setting voltages on the poletips controllable in 0.01 V steps. This setability requirement will be challenging if the magnet quality requires the higher sextupole correction voltages. Since the poletips are powered in a manner that has midplane symmetry, 12 power supplies should be sufficient for the modes up to duodecapole.

6 Novel Model

While the squirrel-cage model's cylindrical symmetry is a familiar one, it is not necessarily the most optimal for this application. Between the magnetic dipoles in the HRS the beam shape is quite pathological, having an aspect ratio greater than 20:1. Because of the beam size, poletips that are vertically distant from the midplane are not being felt by the beam, particularly for corrections that may only require a few volts applied at the poletip.

The first Uniqueness Theorem of Electromagnetism provides that the solution to Laplace's equation in some volume $\mathcal{V}$ is uniquely determined if the potential is specified on the boundary surface $\mathcal{S}$ [13]. Since the harmonics in the multipole expansion are often expressed in cylindrical coordinates, and since the transverse shape of a beam is generally round, it is no surprise that electrostatic correctors are often designed using a cylindrical symmetry that matches a cylinder shaped volume with a potential specified on the outer surface. This is not the only approach to the problem. A rectangular or ellipsoidal volume could be used as well. As long as the surface boundary potential produces the same potential in the midplane, the solutions are unique and identical.

To apply this principle to the novel multipole corrector, we begin by converting the coordinates for the multipole expansion from cylindrical to Cartesian (maintaining z as the longitudinal direction, and x and y representing the transverse dimensions). For the sextupole term, this yields:

$$V_{\mathrm{sext}\,(y=0)} = M(z)_{3,3}(x^3 - 3xy^2) \tag{3}$$

which in the midplane (y = 0) reduces to a cubic equation:

$$V_{\mathrm{sext}\,(y=0)} = M(z)_{3,3}x^3 \tag{4}$$

where $M(z)_{3,3}$ represents the multipole strength parameter [14].

A novel model of a multipole designed using OPERA attempts to implement this theory, creating the specified potential to produce the same fields as the cylindrical model. In this design, the poletips are located 7.5 cm above and below the midplane and 20 cm to the right and left of the optical axis. Since the poletips will have a constant voltage applied to them, placing them some distance for the beam is desired to minimize the variations in potential between the poletips felt by ions in the beam. A profile of the ground-box and poletips arrangement is shown in Figure 13. The spacing between poletips is quite small (5 mm) since the variation in potential is also small, reducing the issue of sparking. The poletips for this novel model were arbitrarily chosen to be 20 cm in length and a rectangular ground-box was placed about the corrector.

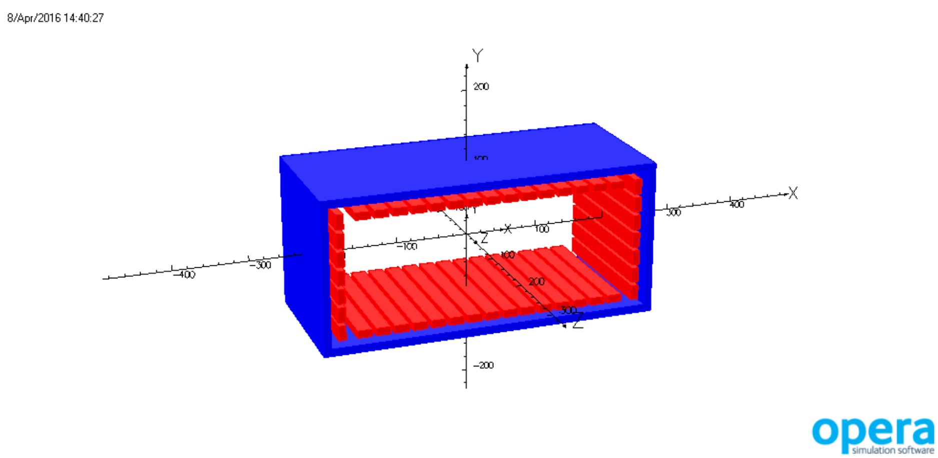

Figure 13: Profile of the Novel multipole corrector.

To determine the voltage to apply to each poletip, the multipole expansion for the desired mode is used. For example, the voltage chosen for each poletip in sextupole mode is calculated using the center of the interior face of the poletip relative to the optical axis using equation (3). The potentials (scaled by an arbitrary factor to represent the multipole strength) applied to the top row of poletips (7.5 cm above the midplane) is shown in Figure 14. Voltages are added for different combined modes. The scaling for the poletips in sextupole and octupole modes is included in Appendix A.

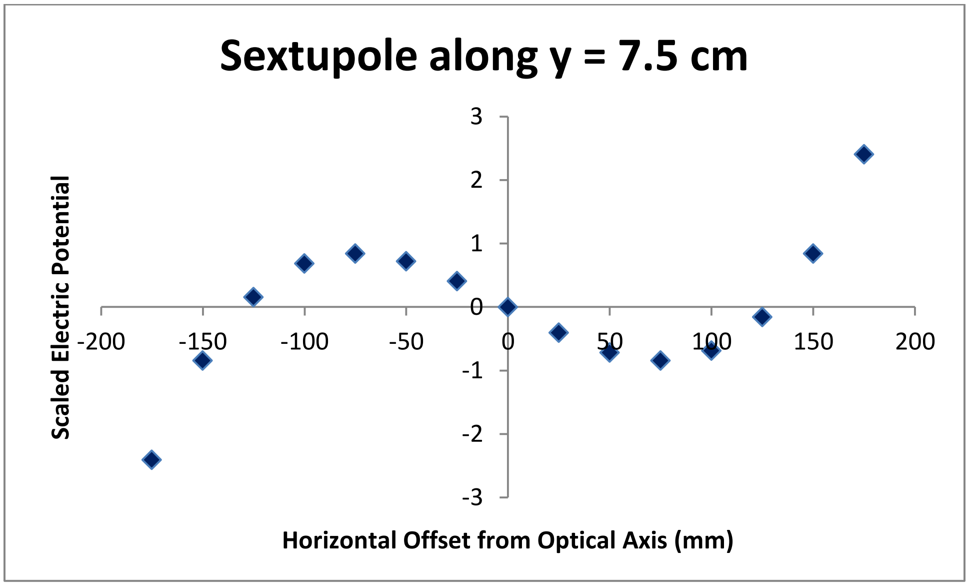

Figure 14: Horizontal variation in electric potential for a sextupole along a line parallel to the midplane and offset by 7.5 cm.

Comparing Figures 10 and 15, we see that the transverse potential variation between the Novel and Squirrel-cage models in the same rectangular region is visually similar. For a more analytical comparison, the potential data from the OPERA model along a line in the center of the element (y=z=0) was plotted as a function of horizontal offset from the optical axis and compared to the ideal sextupole expressed in equation (4). The results, as shown in Figure 16(a), are nearly identical. A similar comparison for the octupole mode is shown in Figure 16(b).

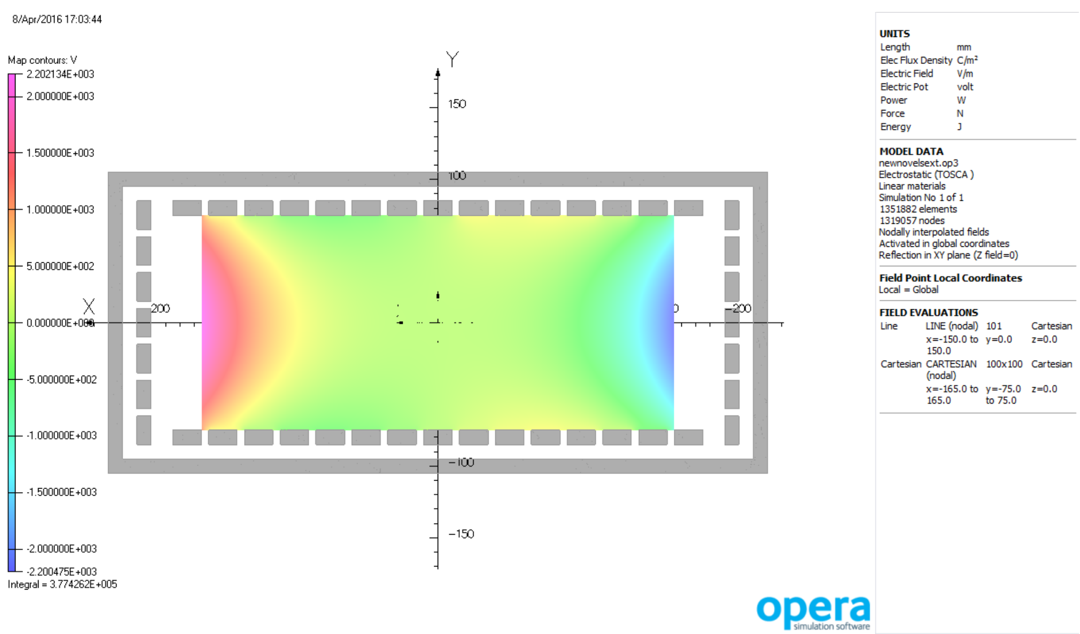

Figure 15: Profile of the electric potential for the sextupole mode of novel corrector.

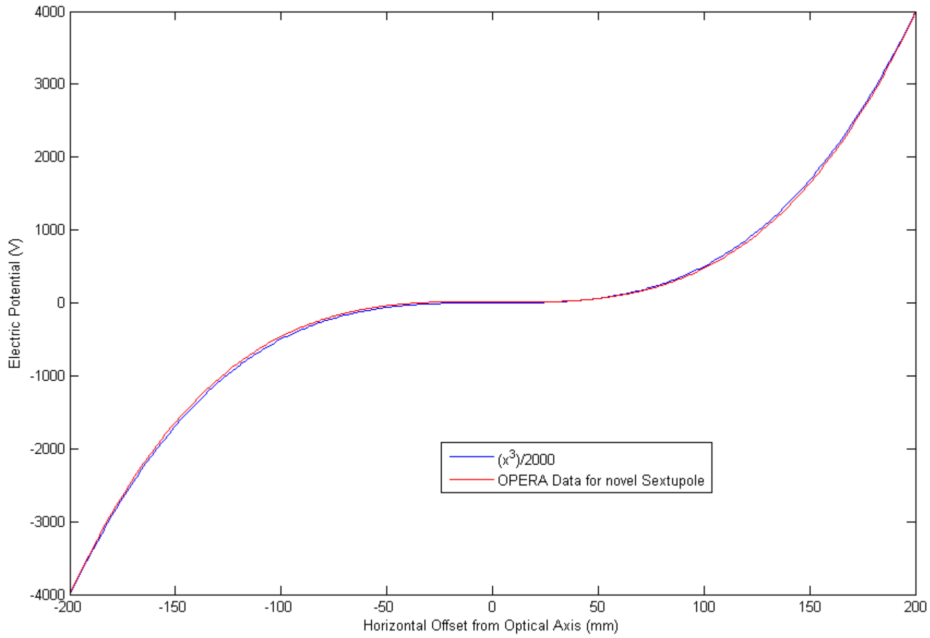

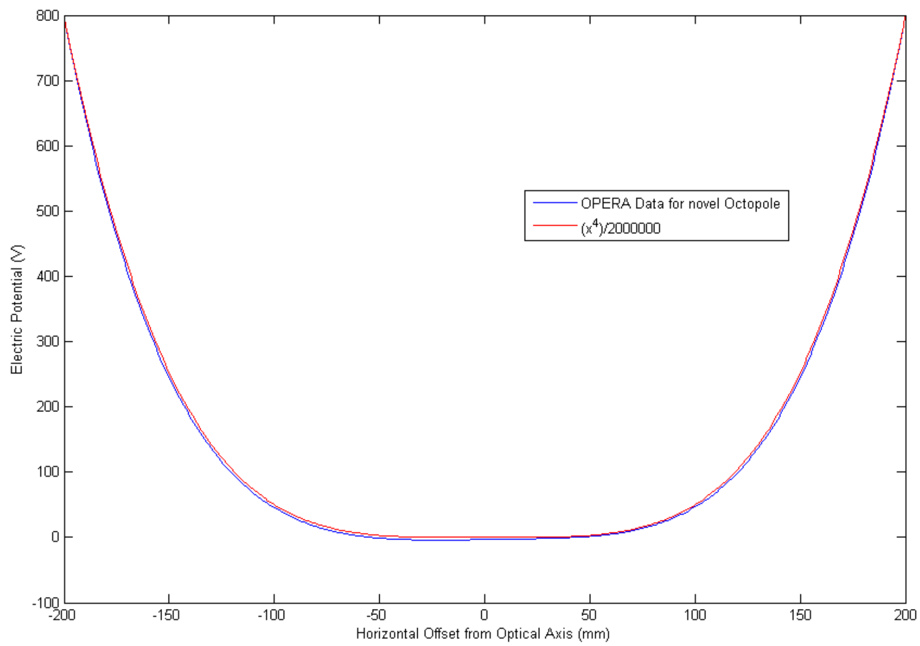

Figures 16(a-b): Comparison of novel OPERA corrector to ideal (a - top) sextupole and (b - bottom) octupole potential along a horizontal line in the midplane in the center of the corrector (y = z = 0).

The midplane potential data map produced for this model was then imported into COSY using the previously described procedure. The transfer maps through 4th order for the sextupole or octupole modes between the cylindrical and novel corrector designs. The effect of correcting the sextupole edge curvature error and octupole correction with the novel corrector is shown in Figure 17(a-b).

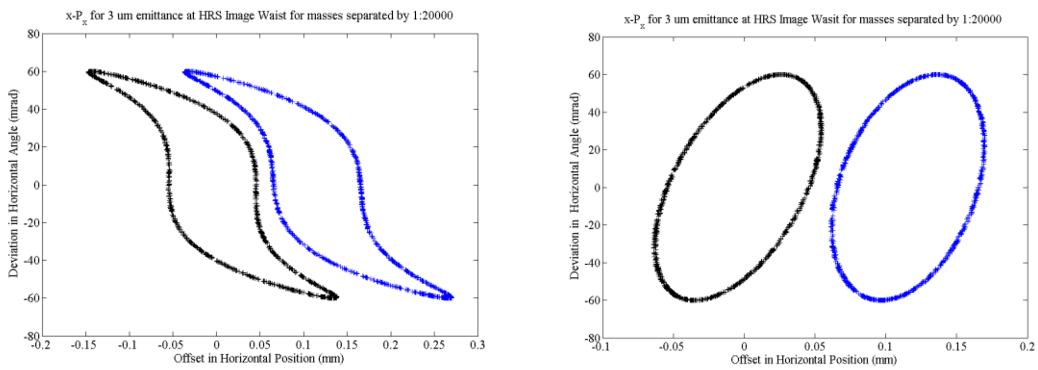

Figure 17(a-b): Horizontal Phase Space at HRS Image Waist for two masses separated by 1:20000 with (a - left) only 2nd order correction and (b - right) 3rd order correction using OPERA model of novel correction in sextupole model.

The potential map data for this novel model was output into COSY and compared with the transfer maps for the squirrel-cage model and COSY's internal model. They were found to be generally comparable, although there is a slight "feed-down" effect in the maps that is originating in the OPERA itself rather than the novel design. In particular the linear imaging term (a|x) was slightly increased and accounts for the rotation of the ellipse from upright seen in Figure 17(b). Higher order multipole modes can also be produced using the same process described for the sextupole.

Further optimization of this model is quite possible. The size of the corrector was chosen so the poletips were far away from the beam, but the variations between this model and the ideal model would seem to allow a much smaller corrector with poletips closer to the beam based on the results shown in Figure 16. Additionally, changing the rectangular shape of the ground box to an ellipse, or modifying the shape and/or number of the poletips is possible. The design shown here fits within the same size vacuum chamber as the squirrel-cage model, but if the size was reduced, a smaller vacuum chamber between the dipoles is possible.

This design also has a potential advantage over the squirrel-cage relative to the 10-pole corrector mode. The squirrel-cage design uses only 24 poletips, a number divisible by 6, 8 and 12. This allows the 6, 8 and 12 pole corrections to function closer to an ideal mode. The 10 pole mode, however, will lack this symmetry. The novel design can, however, apply voltages to create a 10-pole correction (decapole) that is closer to the ideal case. Powering this corrector, however, is a more complicated task. Given the symmetry of how the poletips are powered, it should be possible to use a system of 12 power supplies, but the design of this aspect of the corrector will be a more challenging task. In the current design, the voltage range for the poletips is of the same order as the squirrel-cage model. Reducing the size of the model would reduce the poletip voltages proportionally.

7 Conclusions

The potential map modelling methodology has been benchmarked and shown to be consistent through at least 3rd order with the internal elements used in COSY. Using this new methodology, two potential models have been developed that would function within the requirements of the CANREB HRS multipole corrector.

The first option, the squirrel-cage mode, uses known cylindrical symmetry, making the poletip voltages fairly easy to calculate. Because the higher order modes have a greater influence on the beam closer to the poletips, this model would require a large radial aperture relative to the beam size (~2:1).

Since the electric potential set by the applied voltage for each poletip can be accurately set to match the exact multipole mode desired, the novel model allows for a corrector with poletips much closer to the beam itself. This could possibly reduce the size of the space needed to accommodate the corrector in the vacuum chamber. It also allows for very precise corrections order by order if the setability requirements for the poletip voltages can be met. The lack of cylindrical symmetry means calculating the voltages for each poletip is more complicated, but still reducible to an analytic function. Also, the voltages on the left and right sides of the corrector tend to be comparable the poletip voltages for the squirrel-cage model, but still well under a 2 kV operational limit. Since the poletips maintain voltage symmetry above and below the midplane (i.e. the corresponding poletips on the top and bottom rows are the same), it is anticipated that the number of power supplies needed for this model is similar to the squirrel-cage option.

Both models should be capable of meeting the HRS corrector requirements, and the costs for construction and operation should be comparable. The novel model, if properly designed, should allow more precise aberration correction and is more naturally shaped to the input beam. Additionally, the novel design offers a demonstration of new approach to multipole correction that is scientifically significant.

8 References

[1] K. Makino and M. Berz, COSY Infinity Version 9, Nucl. Instr. Meth. A558 (2005) 346-350.

[2] OPERA-3D, Software for Electromagnetic Design, COBHAM, plc., http://magnet-design-software.com/product/.

[3] R. Baartman, End Effects of Beam Transport Elements (July 2001).

[4] R. Baartman, Intrinstic Third Order Aberrations in Electrostatic and Magnetic Quadrupoles, arXiv:1508.00058v1 (August 1 2015).

[5] J.A. Maloney, New Electrostatic Element Procedures for COSY Infinity, TRI-BN-14-03 (2014).

[6] J.A. Maloney et al., Electrostatic Potential Map modelling with COSY Infinity, Nucl. Instr. Meth. B (2015) http://dx.doi.org/10.1016/j.nimb.2015.12.005.

[7] M. Berz and K. Makino, COSY Infinity 9.1 Beam Physics Manual (2011).

[8] Private correspondence with G. Savard (11/27/2013) and drawing of 48 pole lens assembly.

[9] R. Baartman, Electrostatic Multipole Shapes, TRI-DN-95-23 (August 1995).

[10] R. Baartman Quadrupole Shapes, Phys. Rev. ST-AB, 15, 074002 (2012).

[11] Private correspondence with George Clark (8/9/2015) and drawing Vacbox_Exit_150908.pdf

[12] HRS Design Note TRI-DN-14-06 (2015)

[13] J. Jackson, Classical Electrodynamics, 3rd Edition (1999) pp. 37-38.

[14] M. Berz, Introductory Beam Physics, pp 23-27.

APPENDIX A:

Table of poletip voltage scaling for the squirrel-cage corrector:

Sextupole poletip voltage: #V_sext
Octupole poletip voltage: #V_octo
Decapole poletip voltage: #V_deca
Duodecapole poletip voltage: #V_dodec

#V_pt0 represents a poletip in the midplane (y = 0)

#V_pt0 #V_sext + #V_octu
#V_pt1 (.7071*#V_sext)
#V_pt2 -#V_deca - #V_dodec
#V_pt3 -(.7071*#V_sext) - #V_octu
#V_pt4 -#V_sext + #V_dodec
#V_pt5 -(.7071*#V_sext) + #V_deca
#V_pt6 #V_octo-#V_dodec
#V_pt7 (.7071*#V_sext) - #V_deca
#V_pt8 #V_sext+#V_dodec
#V_pt9 (.7071*#V_sext) - #V_octu
#V_pt10 #V_deca - #V_dodec
#V_pt11 -(.7071*#V_sext)
#V_pt12 -#V_sext + #V_octo - #V_deca + #V_dodec
#V_pt13 -(.7071*#V_sext)
#V_pt14 #V_deca + #V_dodec
#V_pt15 (.7071*#V_sext) - #V_octu
#V_pt16 #V_sext+#V_dodec
#V_pt17 (.7071*#V_sext) - #V_deca
#V_pt18 #V_octo - #V_dodec
#V_pt19 -(.7071*#V_sext) + #V_deca
#V_pt20 -#V_sext+#V_dodec
#V_pt21 -(.7071*#V_sext) - #V_octu
#V_pt22 -#V_deca - #V_dodec
#V_pt23 (.7071*#V_sext)

Table of poletip voltage scaling for the novel corrector (number from left to right horizontally and bottom to top vertically):

#V_toppt1 -2.40625*#V_sext-0.06406*#V_octu
#V_toppt2 -0.84375*#V_sext-0.22148*#V_octu
#V_toppt3 0.15625*#V_sext-0.25156*#V_octu
#V_toppt4 0.6875*#V_sext-0.20586*#V_octu
#V_toppt5 0.84375*#V_sext-0.12656*#V_octu
#V_toppt6 0.71875*#V_sext-0.04648*#V_octu
#V_toppt7 0.40625*#V_sext+0.01938*#V_octu
#V_toppt8 0.0*#V_sext+0.031641*#V_octu
#V_toppt9 -0.40625*#V_sext+0.01938*#V_octu
#V_toppt10 -0.71875*#V_sext-0.04648*#V_octu
#V_toppt11 -0.84375*#V_sext-0.12656*#V_octu
#V_toppt12 -0.6875*#V_sext-0.20586*#V_octu
#V_toppt13 -0.15625*#V_sext-0.25156*#V_octu
#V_toppt14 0.84375*#V_sext-0.22148*#V_octu
#V_toppt15 2.40625*#V_sext-0.06406*#V_octu
#V_botpt1 -2.40625*#V_sext-0.06406*#V_octu
#V_botpt2 -0.84375*#V_sext-0.22148*#V_octu
#V_botpt3 0.15625*#V_sext-0.25156*#V_octu
#V_botpt4 0.6875*#V_sext-0.20586*#V_octu
#V_botpt5 0.84375*#V_sext-0.04648*#V_octu
#V_botpt6 0.71875*#V_sext+0.01938*#V_octu
#V_botpt7 0.40625*#V_sext+0.031641*#V_octu
#V_botpt8 0.0*#V_sext+0.01938*#V_octu
#V_botpt9 -0.40625*#V_sext+0.01938*#V_octu
#V_botppt10 -0.71875*#V_sext-0.04648*#V_octu
#V_botpt11 -0.84375*#V_sext-0.12656*#V_octu
#V_botpt12 -0.6875*#V_sext-0.20586*#V_octu
#V_botpt13 -0.15625*#V_sext-0.25156*#V_octu
#V_botpt14 0.84375*#V_sext-0.22148*#V_octu
#V_botpt15 2.40625*#V_sext-0.06406*#V_octu
#V_leftpt1 -4.625*#V_sext+0.281641*#V_octu
#V_leftpt2 -6.5*#V_sext+1.00625*#V_octu
#V_leftpt3 -7.625*#V_sext+1.450391*#V_octu
#V_leftpt4 -8.0*#V_sext+1.6*#V_octu
#V_leftpt5 -7.625*#V_sext+1.450391*#V_octu
#V_leftpt6 -6.5*#V_sext+1.00625*#V_octu
#V_leftpt7 -4.625*#V_sext+0.281641*#V_octu
#V_rightpt1 4.625*#V_sext+0.281641*#V_octu
#V_rightpt2 6.5*#V_sext+1.00625*#V_octu
#V_rightpt3 7.625*#V_sext+1.450391*#V_octu
#V_rightpt4 8.0*#V_sext+1.6*#V_octu
#V_rightpt5 7.625*#V_sext+1.450391*#V_octu
#V_rightpt6 6.5*#V_sext+1.00625*#V_octu
#V_rightpt7 4.625*#V_sext+0.281641*#V_octu

APPENDIX B:

Beam envelope plots (produced with OPTIM X) for pure separator section of the HRS with a 3 um (above) and 6 um (below) input emittance.